Presubicular VIP expressing interneurons receive facilitating excitation from anterior thalamus

Mérie Nassar, Louis Richevaux, Dongkyun Lim, Dario Tayupo, Erwan Martin, Desdemona Fricker

Neuroscience xxx (xxxx) xxx

Contents lists available at ScienceDirect

Neuroscience

journal homepage: www.elsevier.com/locate/nsc

Presubicular VIP expressing interneurons receive facilitating excitation from anterior thalamus

Mérie Nassar [1,*], Louis Richevaux [1], Dongkyun Lim, Dario Tayupo, Erwan Martin, Desdemona Fricker [*]

Université Paris Cité, CNRS UMR 8002, Integrative Neuroscience and Cognition Center, F-75006 Paris, France

ARTICLE INFO

Keywords:
Interneurons
Patch clamp
Electrophysiology
Presubiculum
Postsubiculum
Head direction

ABSTRACT

The presubiculum is part of the parahippocampal cortex and plays a fundamental role for orientation in space. Many principal neurons of the presubiculum signal head direction, and show persistent firing when the head of an animal is oriented in a specific preferred direction. GABAergic neurons of the presubiculum control the timing, sensitivity and selectivity of head directional signals from the anterior thalamic nuclei. However, the role of vasoactive intestinal peptide (VIP) expressing interneurons in the presubicular microcircuit has not yet been addressed. Here, we examined the intrinsic properties of VIP interneurons as well as their input connectivity following photostimulation of anterior thalamic axons. We show that presubicular VIP interneurons are more densely distributed in superficial than in deep layers. They are highly excitable. Three groups emerged from the unsupervised cluster analysis of their electrophysiological properties. We demonstrate a frequency dependent recruitment of VIP cells by thalamic afferences and facilitating synaptic input dynamics. Our data provide initial insight into the contribution of VIP interneurons for the integration of thalamic head direction information in the presubiculum.

Introduction

The presubicular cortex, located between the hippocampus and the medial entorhinal cortex, plays a crucial role in spatial navigation. Most presubicular neurons signal head direction (HD) (Taube et al., 1990; Boccara et al., 2010; Preston-Ferrer et al., 2016). They fire persistently when the head of an animal is oriented in a specific direction, and they transmit directional information to the medial entorhinal cortex (McNaughton et al., 2006; Langston et al., 2010, Winter et al., 2015, Tukker et al., 2015, Preston-Ferrer et al., 2016).

Recent work has revealed how thalamic HD signals converge with retrosplenial inputs in the presubicular cortex (Richevaux et al., 2023), and the properties of the local microcircuit (Duszkiewicz et al., 2024; Nassar et al., 2015; Peng et al., 2017; Simonnet et al., 2013). Thalamic inputs differentially affect presubicular neurons: layer 3 pyramidal neurons and fast-spiking parvalbumin-expressing interneurons are directly and monosynaptically activated, with strong initial responses, whereas somatostatin-expressing interneurons are indirectly excited, with activity dependent, facilitating dynamics. Feedforward inhibition is largely mediated by parvalbumin interneurons, and may enforce temporally precise head direction tuning during head turns (Nassar et al., 2018). In contrast, feedback and lateral inhibition mediated by Martinotti type somatostatin expressing interneurons onto principal neurons may help sustain firing in head direction cells (Simonnet et al., 2017; Simonnet and Fricker, 2018). In addition to interneurons expressing parvalbumin (PV), somatostatin (SST), another major subtype of GABAergic neurons expresses vasoactive intestinal peptide (VIP) (Kepecs and Fishell, 2016). The intrinsic properties and the functional role of presubicular VIP interneurons have not yet been investigated.

VIP interneurons form a population that is largely non-overlapping with PV and SST interneurons, representing 15 % of total interneurons (Hajos et al., 1996; Xu et al., 2010; Rudy et al., 2011; Tremblay et al., 2016). The cellular diversity even within the population of VIP expressing neurons is high, in the hippocampus and in the neocortex (Tyan et al., 2014; Topolnik and Tamboli, 2022). A recent large-scale study classified cortical VIP interneurons into 5 morpho-electric transcriptomic (MET) types (Gouwens et al., 2020). The connectivity motifs of VIP neurons encompass both inhibition of principal cells and

* Corresponding authors.
E-mail addresses: merie@naox-technologies.com (M. Nassar), desdemona.fricker@u-paris.fr (D. Fricker).
[1] Equally contributing.

https://doi.org/10.1016/j.neuroscience.2024.09.032
Received 8 February 2024; Accepted 16 September 2024
Available online 23 September 2024

inhibition of other interneurons (Acsády et al., 1996; Booker & Vida, 2019). The latter leads to VIP mediated disinhibition of principal glutamatergic neurons and has received much attention in various brain areas (Pi et al., 2013; Jackson et al., 2018; Krabbe et al., 2019; Williams and Holtmaat, 2019) including in the hippocampus (Turi et al., 2019; Wei et al., 2021). The disinhibitory influence of VIP interneurons on the circuit is largely thought to arise from their inhibition of SST interneurons and, to a lesser extent of PV interneurons (Pfeffer et al., 2013; Pi et al., 2013; Karnani et al., 2014; Karnani and Jackson, 2018; Apicella and Marchionni, 2022). Inhibitory-to-inhibitory synaptic interactions among VIP, SST and PV interneurons may help maintain a balance between inhibition and disinhibition, and help flexible computation (Millman et al., 2020; Sadeh and Clopath, 2021). The presubicular HD signaling may also be dependent on VIP interneuron activity. Specifically, VIP interneurons may be key for shaping the multisensory HD signal integration and HD signal updating. To investigate the role of VIP interneurons *in vitro* and in future *in vivo* studies, we need to be able to selectively target them for recording or manipulating.

Here we examined the VIP Cre mouse line (Taniguchi et al., 2011) for its specificity in labeling VIP interneurons in the presubiculum. We characterized the distribution and densities of VIP interneurons across presubicular layers, and characterized the phenotypic diversity of presubicular VIP interneurons in patch clamp recordings in slices. Unsupervised cluster analysis based on the intrinsic electrophysiological properties of VIP interneurons, compared to pyramidal neurons, let us separate three distinct groups. Photostimulation experiments indicate that at least a subset of VIP interneurons can be directly recruited by thalamic inputs, with strongly facilitating dynamics.

Methods

Animals

Experiments were performed on wild-type and transgenic C57Bl6 mice. VIP-Cre mice (Jax n010908, Taniguchi et al., 2011) were crossed with the Ai14 Cre reporter line (Jax n007914, Madisen et al., 2010). Cre mediated recombination resulted in the expression of red fluorescent tdTomato labeling in subsets of GABAergic neurons. VIPcre::tdTomato mice specifically express the red fluorescent protein tdTomato in VIPcre expressing neurons, enabling their visualization in brain slices. Previous studies showed a preferential paternal transmission of the Cre recombinase in the case of PVcre and SSTcre animals (Nassar et al., 2015). Here we bred male homozygous VIPcre mice with females homozygous for tdTomato, to study their offspring of both sexes. Animal care and use conformed to the European Community Council Directive of September 22, 2010 (2010/63/EU) and French law (87/848).

Viral vectors

Viral vectors were injected to induce expression of Chronos, a modified opsin with fast kinetics (Klapoetke et al., 2014). AAV5.Syn.Chronos-GFP.WPRE.bGH (AAV5-Chronos, Penn Vector Core, Addgene 59170P) was used to express this blue light sensitive opsin fused to GFP, under the control of the Synapsin promoter. Viral vectors were stored in aliquots at −80 °C until use.

Stereotaxic surgery

Mice, of age 30–45 days, were anesthetized intraperitoneally with ketamine hydrochloride and xylazine (100 and 15 mg/kg, respectively) and placed in a stereotaxic frame. Unilateral viral injections were performed as described previously (Mathon et al., 2015). AAV injections were targeted to ATN using coordinates from bregma of lateral, 0.75 mm; posterior, 0.82 mm; and depth, 3.2 mm. Injections were made with a Hamilton syringe using a syringe Pump Controller (Harvard Apparatus, Pump 11 elite) at 40 nl/min to deliver volumes of 220 nl AAV5.Syn.Chronos vectors. Leakage from an injection site to surrounding tissue was minimized by withdrawing the pipette slowly after a delay of 10 min. Maximal transgene expression occurred 4 weeks after injection.

Immunohistochemistry

Mice were anesthetized intraperitoneally with ketamine hydrochloride and xylazine (100 and 15 $mg.kg^{-1}$, respectively). They were then perfused transcardially with 0.9 % saline containing heparin (100–200 UI/ml) followed by 30–50 ml of a fixative solution containing 4 % paraformaldehyde in 0.1 M phosphate buffer (PB). Dissected brains were post-fixed 4 h in the same solution at 4 °C, rinsed three times for 3 min, and then placed in a 30 % sucrose solution at 4 °C for at least 24 h. Horizontal sections of thickness 40 μm were cut in 0.1 M PBS using a slicing vibratome (Camdem vibratom 7000smz-2). Membranes were permeabilized by three cycles of freeze-thawing slices on dry ice in a 30 % sucrose containing solution. Sections were washed three times (2 × 30 min, 1 × 60 min) with 0,3% Triton X100 in PBS 0.1 M (BupHTM Phosphate Buffered Saline Packs, Thermo Fisher Scientific), then transferred to a saturation buffer containing 5 % goat serum and 0.3 % Triton X-100 in PBS 0.1 M, and agitated for 2 h at room temperature. Sections were then transferred into the primary antibody solution of 5 % goat serum and 0.3 % Triton X-100 in PBS 0.1 M and gently agitated, overnight at 4 °C. Sections were rinsed three times (2 × 30 min, 1 × 60 min) with 0,3% Triton X100 in PBS 0.1 M, then incubated in dilutions of secondary antibody, conjugated to different fluorophores, overnight at 4 °C under gentle agitation.

4,6-diamidino-2-phenylindole (DAPI, Sigma) was always added to secondary antibodies containing solutions (1:5000) to stain cellular nuclei. For VIP immunostaining, we increased the incubation time with the primary antibody to 48 h and with the secondary antibody to 24 h, both at 4 °C.

The following primary antibody was used: Rabbit Anti-VIP (Immunostar, #20077, 1:500). Secondary antibodies were: Donkey Anti-Rabbit (A647, Jackson ImmunoResearch, 1:500) or Goat Anti-Rabbit (Fisher Scientific, A488, 1:500). Stained sections were mounted on glass slides, coverslipped with anti-fade Prolong Gold (Life technologies).

Image acquisition and analysis

Stained slices were visualized with a confocal microscope (Zeiss LSM710). Presubicular layers and borders were defined using specific cytoarchitectonic features identified by DAPI staining. Images were adjusted for contrast and brightness. For each brain slice, fluorescent tdTomato+ cells from all layers of the presubiculum were identified visually by complete scans of optical sections.

To determine the density of the VIP-INs expressing the tdTomato reporter, we first took Z-stack pictures of the 40 μm thick presubicular sections under the 20x objective of a confocal microscope (Zeiss LSM710). The Cell counter plugin of the ImageJ software was used to count the cells. According to the cell density, the PrS layers were manually and individually selected and their volume was measured (area × range). The density of cells in number/mm3 was determined on n = 53 sections from 6 animals.

Antibody fluorescence was examined for each tdTomato+ cell. A cell was regarded as positive for a given antibody when somatic fluorescence was clearly higher than background levels. Colocalization of antibody labeling was confirmed from observations at all levels of a stack of optical sections for the soma of a neuron. Percentages of single and dual-immuno labeled fluorescent neurons were obtained by dividing the number of immuno-labeled fluorescent neurons by the total number of tdTomato+ neurons. Data are given as mean ± SEM.

Slice preparation and whole cell patch-clamp recordings

Acute slices containing the hippocampus, subicular complex and entorhinal cortex were prepared 4 weeks after AAV5 injections. Animals were anesthetized with ketamine hydrochloride and xylazine mix, treated with 0.1 mL heparin injected intraperitoneally, and perfused intracardially by a cutting solution containing (in mM): 125 NaCl, 25 sucrose, 2.5 KCl, 25 $NaHCO_3$, 1.25 NaH_2PO_4, 2.5 D-glucose, 0.1 $CaCl_2$, 7 $MgCl_2$, cooled to 4 °C, and equilibrated with 5 % CO_2 in O_2. The brain was removed and cut in 300 μm horizontal slices in the same cutting solution with a vibratome (Leica VT1200S). These slices were stored for 15 min in warm (34 °C) ACSF, containing (in mM): 124 NaCl, 2.5 KCl, 26 $NaHCO_3$, 1 NaH_2PO_4, 2 $CaCl_2$, 2 $MgCl_2$, and 11 D-glucose, bubbled with 5 % CO_2 in O_2. Slices were then transferred to a recording chamber (volume 2–3 ml, temperature 33 °C–35 °C) mounted on a BX51WI microscope (Olympus). Experiments were discontinued if transfection at the injection site was weak or if leakage had occurred. The dorsoventral level of horizontal slices that were used for recordings ranged from dorsoventral 2.6 to 3.6 mm with respect to bregma corresponding to the mid to dorsal portion of presubiculum (Paxinos and Franklin, 2013).

Recordings were made with glass pipettes pulled using a Brown-Flaming electrode puller (Sutter Instruments) from borosilicate glass of external diameter 1.5 mm (Clark Capillary Glass, Harvard Apparatus). Electrodes were filled with a solution containing the following (in mM): 135 K-gluconate, 1.2 KCl, 10 HEPES, 0.2 EGTA, 2 $MgCl_2$, 4 MgATP, 0.4 Tris-GTP, 10 Na_2- phosphocreatine, and 2.7–7.1 biocytin. The pH of the pipette solution was adjusted to 7.3 with KOH, and the osmolarity was 290 mOsm. Electrode resistance in the bath, filled with the internal solution, was typically 5–8 MΩ. We used small tip sizes for recording the small GABAergic VIP interneurons (diameter of soma, 10–15 μm). Fluorescent VIP cells were identified using LED illumination with appropriate emission/excitation filters (OptoLED, Cairn Research) using a Luca CCD Camera (Andor). Whole-cell current-clamp recordings were made using a MultiClamp 700B amplifier and pCLAMP software (Molecular Devices). Membrane potential signals were filtered at 6 kHz and digitized at 20–50 kHz. VIP-expressing interneurons were red fluorescent cells in slices from VIPcre::tdTomato mice. Pyramidal neurons of layer III were unlabeled principal neurons, identified as cells with a triangular or ovoid shaped soma. We included them as an external reference population (data from Richevaux et al., 2023). Successful recordings were defined by a high seal resistance above 2 GΩ in cell attached mode. Quality criteria for proceeding with whole cell recordings included a stable access resistance (Ra) < 40 MΩ. Ra was estimated in whole cell voltage clamp mode using the instantaneous current change in response to a −10 mV pulse. The seal test mode in pClamp software was used to estimate the access resistance on-line, before switching to current clamp mode. Bridge balance was set automatically (MultiClamp Commander Software Interface) and monitored throughout the recording. For changes >20 % the recording was discarded. Action potentials needed to be overshooting above 0 mV.

Electrophysiological analysis

Cells intrinsic properties were analyzed as described previously (Huang et al., 2017). Cellular parameters were measured at least 3–5 min after whole-cell records were established. RMP was measured at the beginning of the recording over at least 10 s. Then the membrane potential was kept at −65 mV, for all cells, using a constant current injection as necessary. Electrophysiological parameters were measured from responses to step current injections of 800 ms duration, in VIP interneurons and in principal cells, in a standardized manner. Injected currents increased from negative to positive values, with a range of amplitudes that resulted in hyperpolarization to about −100 mV during the first step and depolarizations close to the maximum sustained firing frequency (evident as noticeably reduced spike amplitudes at the end of the step). Depending on the resistance of the recorded neuron, the first hyperpolarizing step was in the range of −50 pA to −200 pA with an incremental step change of 1/10th of the initial value. Neuronal input resistance R_{in} was determined as the slope of the current–voltage (I-V) relationship between −75 and −55 mV. Membrane time constants (τ) were estimated from a double exponential fit to the negative deflection of membrane voltage (Levenberg–Marquardt algorithm; Golowasch et al., 2009) in response to a 800 ms hyperpolarizing current injection inducing a voltage change of up to 10 mV. A "sag ratio," indicative of Ih expression, was calculated for steps in which the voltage deflection reached values between −105 and −90 mV, as the ratio of the maximal negative potential, typically from 0 to 200 ms, divided by the mean steady state voltage deflection, between 400 and 800 ms.

Action potentials of amplitude at least 20 mV were detected from continuous periods of rising membrane potential. Rheobase (or threshold current for firing) was defined as the smallest positive current step of 800 ms that elicited at least one AP. Firing frequency (Hz) was deduced by dividing the number of APs over time (APs/sec). Input–output (I–O) curves were constructed by plotting firing frequency (APs/sec) as a function of injected current. The I–O gain was measured from a linear fit to frequencies measured from the 4 current steps after rheobase. First AP latency was calculated from the first AP elicited, at latency less than 100 ms. Action potential waveform features were obtained by averaging the measures from the first AP elicited, on the rheobase current step, at latency less than 100 ms. AP threshold (threshold) was defined as the membrane potential when $dV/dt > 35$ mV/ms. AP peak was its maximum potential. The AP rising amplitude (amplitude) was the difference between the threshold and the peak AP voltage. AP width (width) was measured from the half-height of the AP rising phase. Max depolarization rate and max repolarization rate were defined as the maximum and minimum dV/dt, during rising and falling phases of APs, respectively. The AHP was the voltage minimum after the AP peak and its amplitude (AHP) was defined as the difference from the threshold.

Optical stimulations

Chronos-expressing ATN axons were stimulated optically with a single-wavelength LED system (470 nm; Cairn Research OptoLED) connected to the microscope via a custom-made triple port (Cairn Research). Synaptic responses of presubicular VIP interneurons were recorded in whole-cell current- or voltage-clamp modes. LED illumination gave a 200 μm diameter spot with a 60 1.0 NA plan-Apochromat objective. Flashes of 0.5 ms were delivered close to recorded somata. We typically used low-intensity stimulation of 0.1– 0.5 mW, set to induce near threshold responses, reducing network activation after ATN axon stimulation. Excitatory and inhibitory postsynaptic responses were evoked by 10 Hz, 30 Hz and 70 Hz stimulus trains. We tested for monosynaptic excitation by stimulating in the presence of TTX (1 μM; Tocris Bioscience) to block polysynaptic excitation and 100 μM 4-AP (Sigma-Aldrich) to enhance axonal depolarization (Cruikshank et al., 2010; Mao et al., 2011).

Biocytin staining and morphological 3D reconstructions across presubicular layers

VIP interneurons were filled with 0.3–0.4 % biocytin (3–4 mg/ml) during recordings to reveal their morphology post hoc (Nassar et al., 2015; Simonnet et al., 2013). After recording, slices were fixed in 4 % PFA in 0.1 M phosphate buffer at 4 °C for 24 h. Slices were then rinsed in PBS and cryoprotected in 30 % sucrose mixture at 4 °C overnight. Membranes were permeabilized by three cycles of freeze-thawing over dry ice and then washed with PBS. Slices were agitated in a saturation buffer containing 2 % milk powder and 1 % Triton X-100 in PBS 0.1 M for 3 h at room temperature. Then, sections were gently agitated with Streptavidin-Cy5 conjugate (1:500, Molecular Probes) and DAPI in the blocking solution overnight at 4 °C. After washing with PBS, slices were

mounted on coverslips using ProLong Gold Antifade Mountant (Invitrogen). Filled cells were visualized with a confocal microscope (Zeiss LSM710). Neuronal anatomy was derived from z stacks of acquired images (Neurolucida, RRID:SCR_001775; MBF Bioscience).

The presubiculum has a curved trapezoid shape in horizontal sections, and its radial axis is defined by the pyramidal cell apical dendrites. Blood vessels follow the same main orientation. Six presubicular layers were identified based on the following cytoarchitectonic features: Layer I stands out as an almost cell free layer. Layer II possesses a high density of DAPI labeled cell bodies. The beginning of layer II was used to define the proximal border to the subiculum, and the distal end of layer II corresponds to the transition to the parasubiculum. Layer III has a medium cell body density. Anterior thalamic axons ramify across the superficial layers I and III (Fig. 5A; see also Nassar et al., 2018). Layer IV is sparsely populated, it is part of the deep layers, and lies below the thalamo-recipient superficial layers (Richevaux et al., 2023). The deep layers V/VI appear as the continuation of the subiculum.

Statistical analysis

Signals were analyzed with AxoGraphX and custom-written software (Labview, National Instruments; MATLAB, The MathWorks). Algorithms to detect APs and measure active and passive neuronal properties are as described previously (Simonnet et al., 2013; Huang et al., 2017). Results are given as mean ± SEM (number of cells, slices, or animals as indicated). Statistical analysis was performed with Prism (GraphPad Software). The Wilcoxon signed rank test for matched pairs was used to compare nonparametric data in matched samples. A Kruskal–Wallis one-way ANOVA test was followed by Dunn's post hoc test to compare more than two groups. Mann-Whitney non parametric tests were also performed to compare differences between two independent groups. Two-way ANOVA was also used to study the effect of two independent

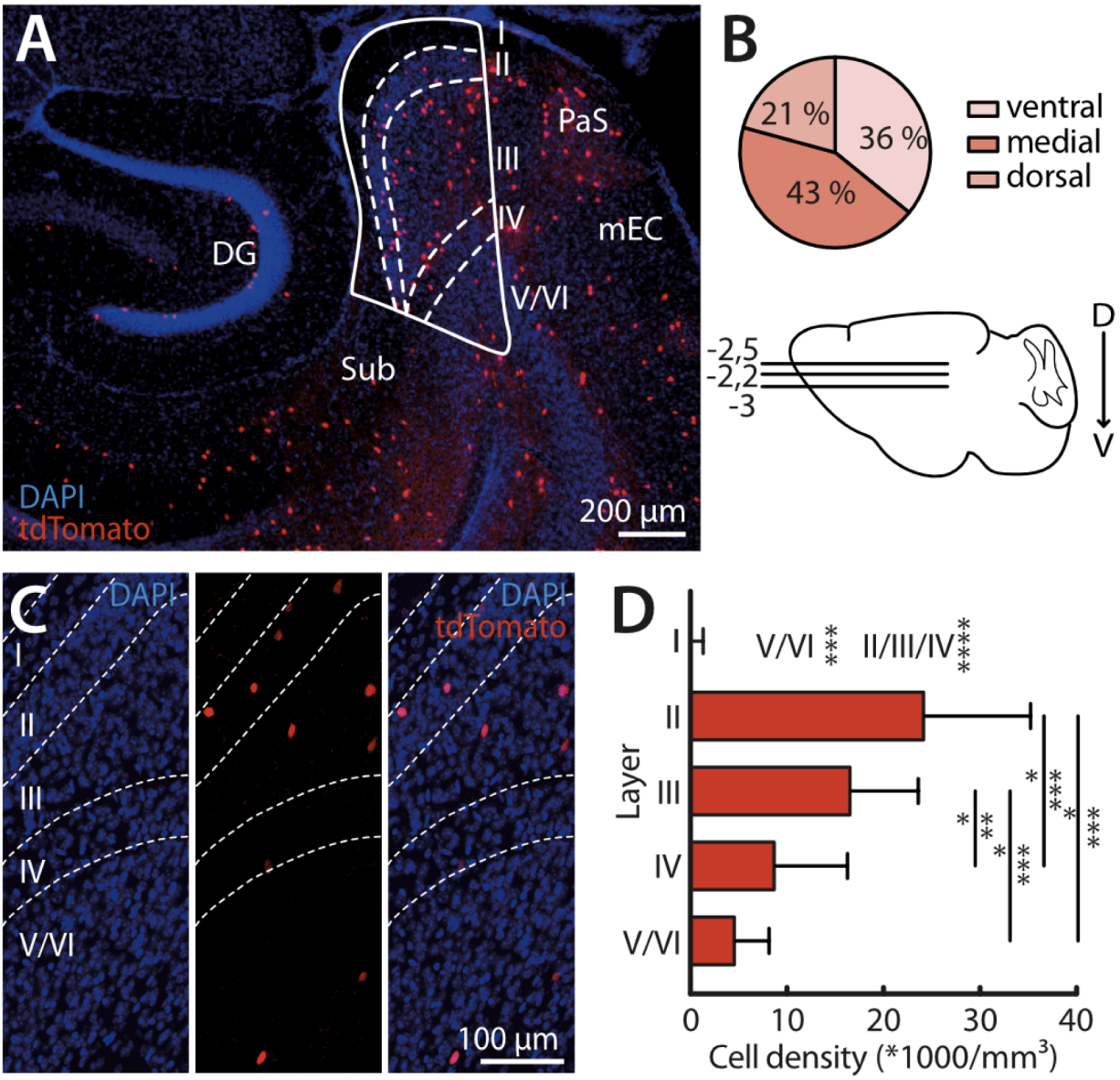

Fig. 1. Layer-specific distribution of VIP interneurons in the presubicular HD cortex A) Horizontal section of the presubiculum with red tdTomato labeled neurons from a VIPcre::tdTomato mouse. The presubiculum continues from the subiculum (Sub), faces the dentate gyrus (DG), and lies adjacent to parasubiculum (PaS) and medial entorhinal cortex (mEC). DAPI staining in blue. B) Slices obtained from different dorso-ventral levels, ranging from −2,2 mm (most dorsal) to −3 mm (most ventral). C) DAPI staining (left, blue), tdTomato labeled VIP interneurons (middle, red), and an overlay (right) of presubicular layers I to V/VI. D) Densities (mean ± SEM) of labeled VIP interneurons in different layers of presubiculum. Data from 10 slices of 3 animals (Kruskal-Wallis test, *** $P < 0.001$, **** $P < 0.0001$). (For interpretation of the references to color in this figure legend, the reader is referred to the web version of this article.)

variables at the same time.

Results

Mouse model validation and layer distribution of VIP interneurons in the presubiculum

We first aimed to confirm the specificity of the VIPcre mouse line (Taniguchi et al., 2011) as a genetic tool for accessing VIP interneurons in presubiculum. To do this, VIPcre mice were crossed with a reporter line expressing a red fluorescent protein, tdTomato (Ai14, Madisen et al., 2010), that let us visualize VIP interneurons in slices. We then examined the distribution of VIP expressing interneurons across the different layers of the presubiculum in these transgenic mice. Fig. 1A shows the presubiculum in the context of the mouse hippocampal formation. Six cytoarchitectonic layers can be recognized. The distribution of fluorescently labeled VIP interneurons was quantified in 19 ventral, 23 medial and 11 dorsal presubicular slices from three animals. (Fig. 1B). VIP interneurons were sparse in layer I (286 ± 143.5). Their density was higher in layer II (24324 ± 1499 cells/mm3) than in layer III (16712 ± 946 cells/mm3). It further decreased in layer IV and even more in layers V/VI. Overall, VIP interneuron density was significantly higher in the superficial layer II and III than in the deep layers, IV and V/VI (Fig. 1C,D).

We then used antibodies against VIP to examine the specificity of labeling in the VIPcre::tdTomato mice (Fig. 2) in superficial layers I-III and in deep layers IV and V/VI of the presubiculum. The tdTomato+ fluorescent presubicular cells that were also immunopositive for VIP were quantified in 8 non-adjacent slices from three animals (Fig. 2A,B). As expected, the great majority of tdTomato+ neurons in the VIPcre line were immunopositive for VIP (393/413). VIP labeling of TdTomato+ cells was even higher in superficial layers (95 ± 1 %) than in deep layers (87 ± 6 %) with no significant difference.

Cluster analysis of electrophysiological parameters reveals groups of presubicular VIP interneurons

We measured passive membrane properties, AP waveforms and firing patterns of 85 presubicular VIP interneurons and compared them to 71 layer III pyramidal neurons. The classification is based on electrophysiological criteria, where pyramidal neurons were used as an external reference for the interneuron containing clusters, in order to define a significant cut-off value for clusters. All recordings were made from neurons in slices from the mid-to-dorsal portion of the presubiculum. Dorso-ventral depths ranged from −3 to −2.2 mm, with most interneurons recorded from a level close to −2.5 mm (cf. Fig. 1B). Fluorescently labeled neurons in VIPcre::tdTomato mice and unlabeled pyramidal neurons in layer III were recorded from male and female mice, and mostly from superficial layers of presubiculum. Unsupervised cluster analysis using Ward's method (Ward, 1963) was based on 13 electrophysiological variables as listed in Table 1. Supplementary Fig. 1 shows these parameters in the space defined by the three first principal components. The hierarchical tree diagram (Fig. 3A) points to the existence of two VIP interneuron containing clusters (Cluster 1 and 2) that were segregated from a cluster containing pyramidal neurons, and a third group of VIP interneurons (Cluster 3). Within-cluster Euclidean distances for clusters 1, 2 and 3 were similar (10, 11 and 15, respectively). We explore VIP interneurons in the three clusters in detail below. All datapoints are plotted for each cell, represented by a dot, for each cluster (Fig. 3F).

Cluster 1: Highly excitable VIP interneurons

Cluster 1 comprised 39 VIP interneurons and one unlabelled neuron. A representative firing pattern of a VIP interneuron with irregular or quasi fast-spiking firing pattern and fast AP is shown (Fig. 3B-D, blue traces). Cluster 1 interneurons typically fired spontaneously both in the whole-cell mode and in cell-attached records made before rupturing the membrane. Their mean RMP was relatively depolarized, similar to VIP interneurons in Cluster 2 and 3 (−53.7 ± 1.7 mV; n = 39; mean ± SEM). Input resistance was particularly high, 1287 ± 108 MΩ, similar to Cluster 2 and significantly higher than for cluster 3 VIP interneurons (Fig. 3E, F). Membrane time constant, tau, was 28 ± 2 ms. Hyperpolarizing current injections induced a moderate voltage sag (Fig. 3B; sag ratio 1.11 ± 0.01). Cluster 1 cells could fire in quasi fast patterns. They were very excitable, and APs were elicited at a very low rheobase current of 10.5 ± 1.0 pA. The maximum firing rate, determined from a subset of n = 7 cells, was 100.2 ± 14.6 Hz. Firing rate gain was 1564 ±

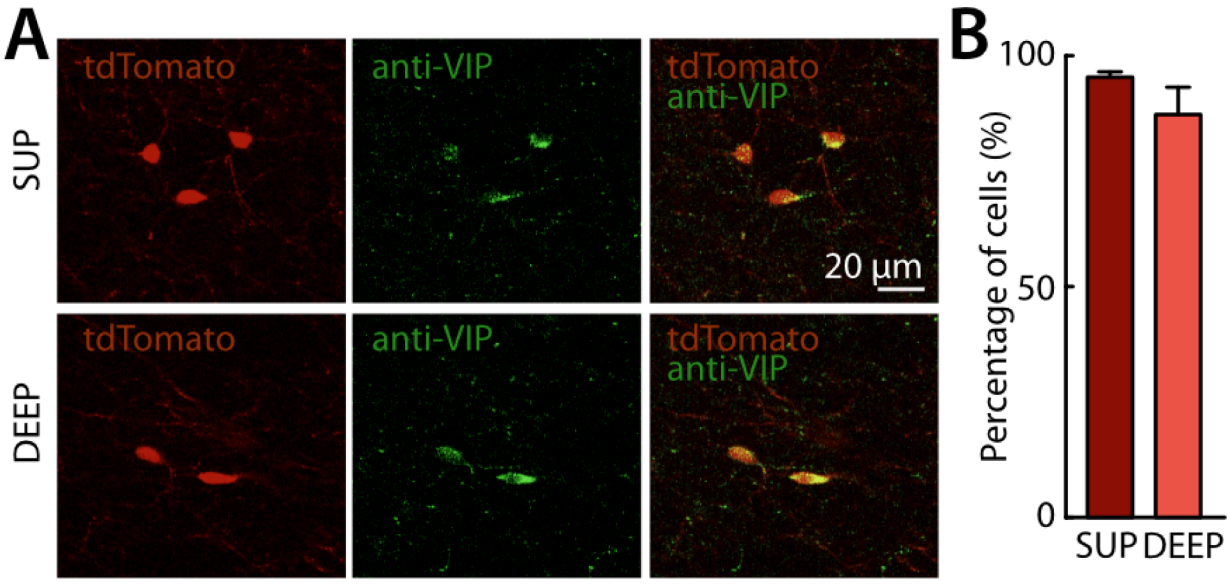

Fig. 2. Immunostaining confirms the specificity of the VIPcre::tdTomato labeling. A) Presubicular sections from VIPcre::tdTomato mice stained with anti-VIP antibody in superficial (SUP, top panels) and deep (DEEP, bottom panels) layers. For each row, tdTomato labeled neurons (red) are on the right, immunostaining against VIP in the middle (green) and merge on the right. B) Bar graphs indicate percentages of antibody labeling of tdTomato+ VIP interneurons (mean ± SEM). Data obtained from 8 slices of 3 animals. (For interpretation of the references to color in this figure legend, the reader is referred to the web version of this article.)

Table 1
Electrophysiological intrinsic properties of 85 presubicular VIP interneurons recorded from the VIPcre::tdTomato mouse line and 71 presubicular layer 3 pyramidal neurons recorded from transgenic or wild-type animals. Using these 13 parameters for Ward's unsupervised cluster analysis let us separate the population of VIP interneurons in two main clusters and a third cluster, composed of both VIP interneurons and pyramidal neurons. Values (mean ± SEM) for each parameter are given for each cluster. p-values indicate statistical differences between clusters and between VIP and pyramidal neurons within cluster 3 and between VIP neurons across the three clusters, calculated using a Mann-Whitney test. Values in green are inferior to 0.05.

	Cluster 1			Cluster 2			Cluster 3									Mann-Whitney test			Mann-Whitney test		
	VIP			VIP			All			VIP			MW	PYR					Cluster 3 VIP only		
	Mean	SEM	N	Mean	SEM	N	Mean	SEM	N	Mean	SEM	N	*p-value*	Mean	SEM	N	Cluster 1-2	Cluster 1-3	Cluster 2-3	Cluster 1-2	Cluster 1-3	Cluster 2-3
Resting membrane potential (mV)	-53.67	1.70	39	-56.34	2.13	29	-69.00	1.19	88	-57.00	1.59	17	3.24E-06	-71.87	1.20	71	2.69E-01	1.35E-09	4.24E-06	2.69E-01	2.53E-01	9.09E-01
Input resistance (MΩ)	1286.63	107.82	39	1163.84	120.71	29	467.19	26.97	88	762.42	77.70	17	1.86E-05	396.50	20.51	71	4.35E-01	3.16E-14	7.93E-12	4.35E-01	3.28E-03	1.49E-02
Tau (ms)	27.95	1.73	39	39.09	2.88	29	25.20	1.01	88	30.03	1.80	17	9.32E-03	24.04	1.14	71	2.38E-03	1.90E-01	8.83E-06	2.38E-03	4.17E-01	7.04E-02
Sag ratio	1.11	0.01	39	1.08	0.01	29	1.09	0.01	88	1.14	0.03	17	7.60E-02	1.08	0.01	71	2.18E-01	6.85E-02	1.90E-01	2.18E-01	7.14E-01	4.22E-01
Rheobase current (pA)	10.50	1.04	39	14.96	1.17	29	47.95	2.93	88	37.09	5.47	17	2.06E-02	50.55	3.33	71	2.97E-03	2.05E-17	6.16E-13	2.97E-03	2.83E-07	4.83E-05
Input-output slope (Hz/nA)	1564.28	138.18	39	836.34	115.38	29	422.30	22.37	88	553.48	84.42	17	1.86E-01	390.89	17.54	71	3.90E-04	1.15E-12	5.38E-02	3.90E-04	1.90E-05	2.75E-01
AP threshold (mV)	-38.82	1.03	39	-33.90	1.02	29	-32.32	0.65	88	-27.25	1.71	17	1.96E-03	-33.54	0.62	71	1.44E-03	8.74E-07	5.16E-01	1.44E-03	6.81E-06	5.50E-03
AP width (ms)	0.45	0.02	39	0.71	0.03	29	0.69	0.03	88	0.61	0.02	17	2.67E-01	0.70	0.03	71	3.63E-10	2.33E-12	5.77E-02	3.63E-10	4.84E-06	3.00E-02
AP AHP (mV)	-20.36	0.69	39	-15.01	0.76	29	-19.19	0.36	88	-18.41	0.94	17	4.37E-01	-19.38	0.39	71	8.50E-06	2.51E-01	5.33E-06	8.50E-06	2.47E-01	1.23E-02
AP amplitude (mV)	74.25	1.13	39	54.22	2.23	29	77.19	0.93	88	69.53	1.55	17	3.76E-06	79.02	0.97	71	1.17E-08	1.37E-02	1.10E-11	1.17E-08	2.20E-02	1.20E-04
AP maximum depolarization rate (V/s)	423.08	14.25	39	220.89	13.34	29	340.36	6.42	88	338.30	16.61	17	4.59E-01	340.85	6.95	71	2.54E-10	7.54E-07	9.35E-10	2.54E-10	8.89E-04	1.25E-05
AP maximum repolarization rate (V/s)	-180.06	7.10	39	-82.00	4.99	29	-117.13	3.37	88	-117.18	4.66	17	9.83E-01	-117.12	4.04	71	9.91E-12	6.91E-13	5.65E-07	9.91E-12	2.15E-07	3.80E-05
Onset latency (ms)	113.04	13.97	39	205.36	28.82	29	148.27	11.64	88	128.43	19.88	17	6.19E-01	153.03	13.62	71	4.88E-03	3.11E-02	1.79E-01	4.88E-03	2.93E-01	2.32E-01

138 Hz/nA. The latency to fire, at rheobase, was 113 ± 14 ms. AP threshold was significantly more negative than in cluster 2 and 3 VIP interneurons, at −38.8 ± 1.0 mV. AP width was significantly shorter than in the other two clusters, 0.45 ± 0.02 ms, and AP amplitude was very high, 74 ± 1 mV. The maximum AP depolarization and repolarization rates were 423 ± 14 V/s and −180 ± 7 V/s, respectively, significantly greater than in other VIP interneurons. Spike AHPs were biphasic (Fig. 3B, C), with mean maximal amplitude of −20.4 ± 0.7 mV.

Cluster 2: VIP interneurons with broad AP waveforms

Cluster 2 comprised 29 VIP interneurons. A representative firing pattern of a VIP interneuron with regular firing pattern and a broad AP waveform is shown (Fig. 3B-D, green traces). Cluster 2 neurons also fired spontaneously with mean RMP −56.3 ± 2.1 mV. Input resistance was also very high, 1164 ± 121 MΩ (Fig. 3E, F). Membrane time constant was significantly higher than in cluster 1 cells (39 ± 3 ms). Hyperpolarizing current injections also induced a moderate voltage sag (Fig. 3B; sag ratio 1.08 ± 0.01). Cluster 2 cells could fire in regular patterns. APs were elicited at a rheobase current of 15.0 ± 1.2 pA, higher than for cluster 1. The maximum firing frequency for a subset of n = 5 neurons was relatively low, 48.3 ± 10.4 Hz. Firing rate gain was 836 ± 115 Hz/nA, about twice lower than for cluster 1. Neurons from cluster 2 had significantly longer onset latencies to fire at rheobase (205 ± 29 ms for cluster 2, Fig. 3F). AP threshold was higher (−33.9 ± 1.0 mV), and AP width was broader than for cluster 1 (0.71 ± 0.03 ms). AP amplitude was 56 ± 2 mV, significantly lower compared to cluster 1 and to cluster 3 VIP interneurons (Fig. 3C-D). The maximum AP depolarization and repolarization rates were significantly slower than for cluster 1 and 3 (221 ± 13 V/s, −82 ± 5 V/s respectively). Spike AHPs were simple (Fig. 3C) and with lower amplitude compared to cluster 1 and 3 neurons (−15.0 ± 0.8 mV, Fig. 3C, D).

Cluster 3: A third group of VIP interneurons with lower input resistance

Cluster 3 was composed mostly of pyramidal neurons (black, n = 71) and also of a third group of VIP interneurons. Representative recordings with firing pattern and AP waveform of a pyramidal neuron and an irregular spiking VIP interneuron are shown (Fig. 3B-D). In the following we focus on this third group of VIP interneurons in cluster 3 (red, n = 17). These interneurons had a mean membrane potential of −57.0 ± 1.6 mV. Most remarkably, their input resistance was 467 ± 27 MΩ, significantly lower than that in cluster 1 and 2 VIP interneurons, but still significantly higher than the pyramidal cells in cluster 3 (Fig. 3E,F). The time constant was 30 ± 2 ms. The voltage sag was similar to the other clusters (1.09 ± 0.00). Rheobase was significantly higher than in the two other clusters, at 37.1 ± 5.5 pA. Firing was often irregular, and the maximum firing frequency for one example neuron of this group was 66 Hz. The input–output slope quantifying the firing rate gain of this VIP interneuron group was 553 ± 84 Hz/nA, lower than in the other two VIP interneuron clusters 1 and 2. Action potential threshold was on average more depolarized than in the other VIP interneuron clusters, at −27.3 ± 1.7 mV. The AP width was 0.61 ± 0.0 ms, more similar to pyramidal neurons and also to cluster 2 VIP interneurons. AP AHPs were −18.4 ± 0.9 mV, intermediate compared to values in cluster 1 and 2. Also the AP amplitudes (69.5 ± 1.6 mV), depolarization rates (338 ± 17 V/s), repolarization rates (−117 ± 5 V/s) and spiking onset latencies (128 ± 20 ms) for cluster 3 VIP interneurons were intermediate compared to the other clusters (cf. Table 1).

Morphology

All recorded VIP interneurons were filled with biocytin to reveal their soma position. Axonal and dendritic morphologies of a sample of 7 well-filled cells were completely reconstructed with Neurolucida. We characterized the morphologies of neurons from the electrophysiologically defined VIP interneuron groups. Fig. 4A shows the axonal and dendritic arborizations of three VIP interneurons from cluster 1, two VIP interneurons from cluster 2 and two from the group of VIP interneurons in cluster 3. The somata of these VIP expressing cells were ovoid, and located in superficial layers II or III. The complexity of neuronal morphologies for the example neurons was overall similar. Dendritic trees were rather short, typically multipolar, ramifying in all directions from the soma. Axons emerged from the soma or from an ascending dendritic trunk. They were dense and possessed extensive arborizations. Their main orientation was perpendicular to the layer organization, innervating both superficial and deep layers, and generally following the radial axis of presubiculum. For one VIP interneuron in cluster 1, axons were oriented toward deep layers only.

Sholl analysis let us quantify the spatial distribution of neurites for each cell (Fig. B-E). Axonal Sholl plots showed a heterogenous distribution of axon intersections, with a peak at a distance of 100 μm from the soma (Fig. 4B). Dendrites occupied a radius of 100–150 μm around the soma and were oriented in all directions (Fig. 4C). The axonal length analysis indicated that most of the axons from the reconstructed VIP interneurons were located in layer III and IV (Fig. 4D), indicating that these neurons target mostly other neurons in layer III. Dendrites were rather short and mostly located in layer III (Fig. 4E).

Anterior thalamic axons terminals directly contact VIP interneurons

We asked whether ATN axons innervate presubicular VIP interneurons using the viral expression of Chronos in the anterior thalamic nuclei. Injection of AAV5-Chronos in the ATN led to the expression of

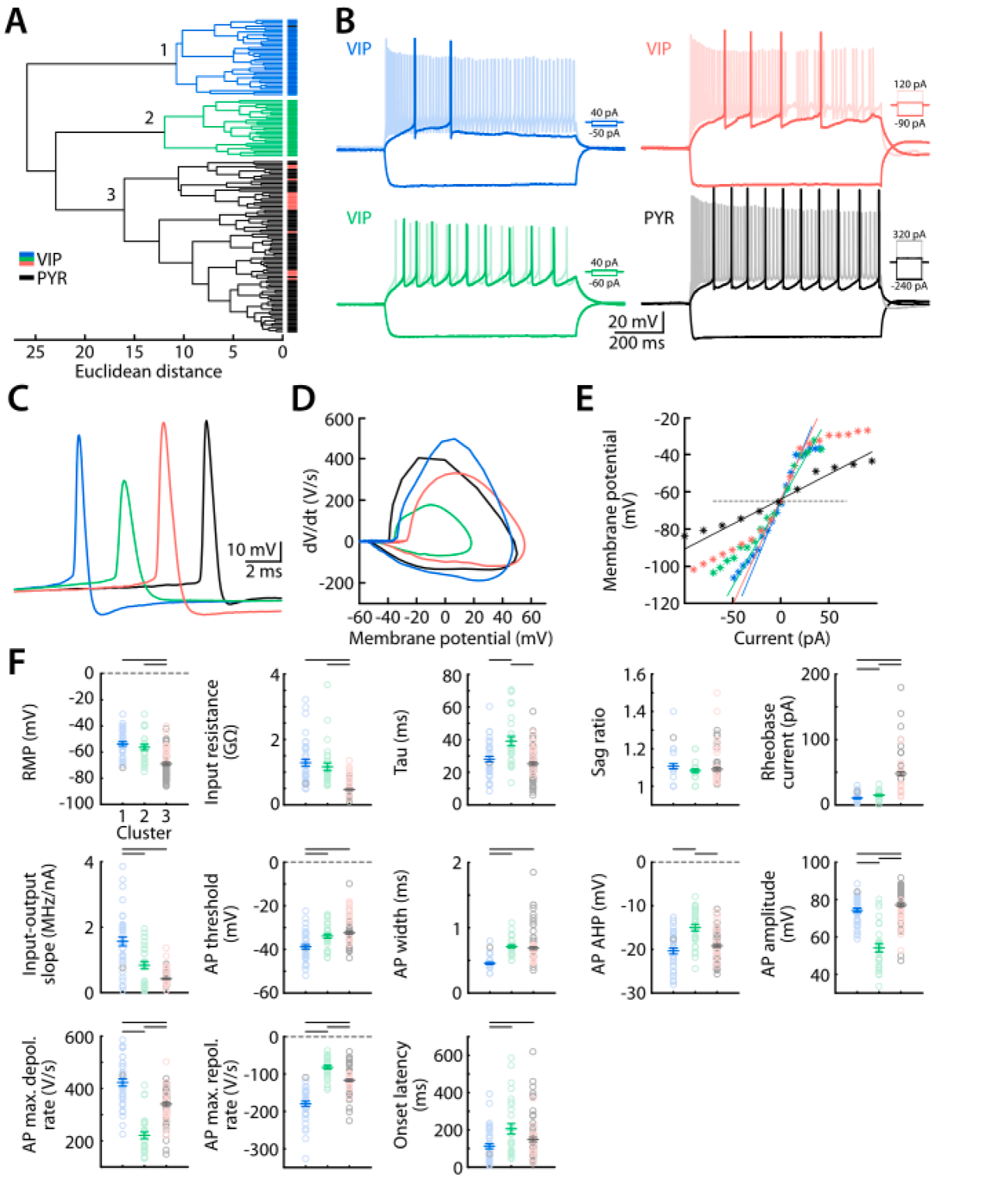

Fig. 3. Cluster analysis classification of presubicular VIP interneurons. A) Unsupervised cluster analysis of 13 parameters, detailed in Table 1, revealed two main subpopulations of VIP interneurons. A cut-off at a Euclidean distance of 16 separated VIP interneurons in Cluster 1 in blue, and Cluster 2 in green, from the Cluster 3 that contains mainly pyramidal cells, in black. A group of VIP interneurons, in red, clustered together with the pyramidal neurons in Cluster 3. B) Representative examples of firing patterns for each cluster and cell type. Neurons were maintained at −65 mV and injected with hyperpolarizing and depolarizing current steps. Voltage responses to hyperpolarizing and rheobase current injections are indicated in full color. C) First action potential waveforms at rheobase and D) the corresponding phase plots. E) Current–voltage relations at subthreshold potentials are plotted for neurons from each cluster. F) The values for active and passive electrophysiological properties are plotted for each neuron (mean ± SEM), as a function of the cluster. Each dot is a neuron. Lines represent significant differences measured by a Mann-Whitney test, complete p-values are detailed in Table 1. (For interpretation of the references to color in this figure legend, the reader is referred to the web version of this article.)

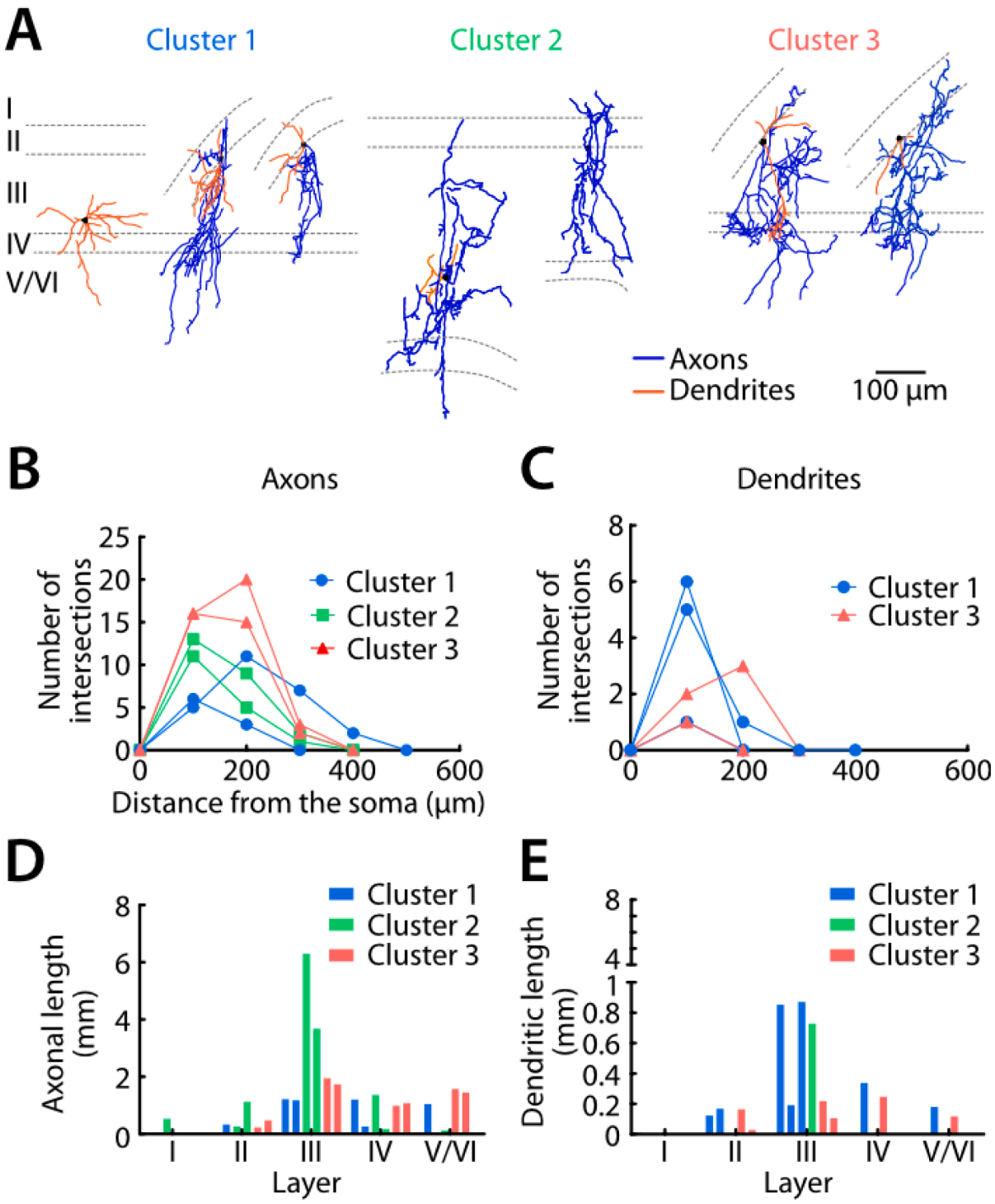

Fig. 4. Axo-dendritic morphology of presubicular VIP interneurons. A) Axo-dendritic arbors of seven biocytin-filled and reconstructed VIP interneurons. They were part of cluster 1 (blue), 2 (green), or the cluster 3 VIP-cell group (red). Axons in blue, dendrites in red, and cell bodies in black. B, C) Sholl plots of the number of axon (left panel) and dendrite (right panel) crossings for concentric circles against distance from the soma for each reconstructed neuron from each cluster. D, E) Axonal (left) and dendritic (right) length per layer for each cluster of neurons. (For interpretation of the references to color in this figure legend, the reader is referred to the web version of this article.)

this modified opsin (Klapoetke et al., 2014), in their axons that form the main afferents to the presubiculum (Simonnet et al., 2017, Nassar et al., 2018, Richevaux et al., 2023). As expected, ATN axons ramified in the superficial layers I and III of the presubiculum, while they were largely absent from layer II and from deep layers. Thus, the main dendritic domain of VIP interneurons overlapped with thalamic axons (Fig. 5A, B).

In *ex vivo* slice recordings, Chronos expressing ATN axons were stimulated by whole field illumination of the presubiculum with a 470 nm blue LED. We found that photostimulation induced excitatory postsynaptic currents (EPSCs) in all recorded superficial layer VIP interneurons. The mean amplitude and delay to EPSC onset was 17.86 ± 3.86 pA and 3.48 ± 0.27 ms respectively (Fig. 5D, n = 11). Responses persisted in the presence of TTX-AP, indicating the excitatory ATN-PrS

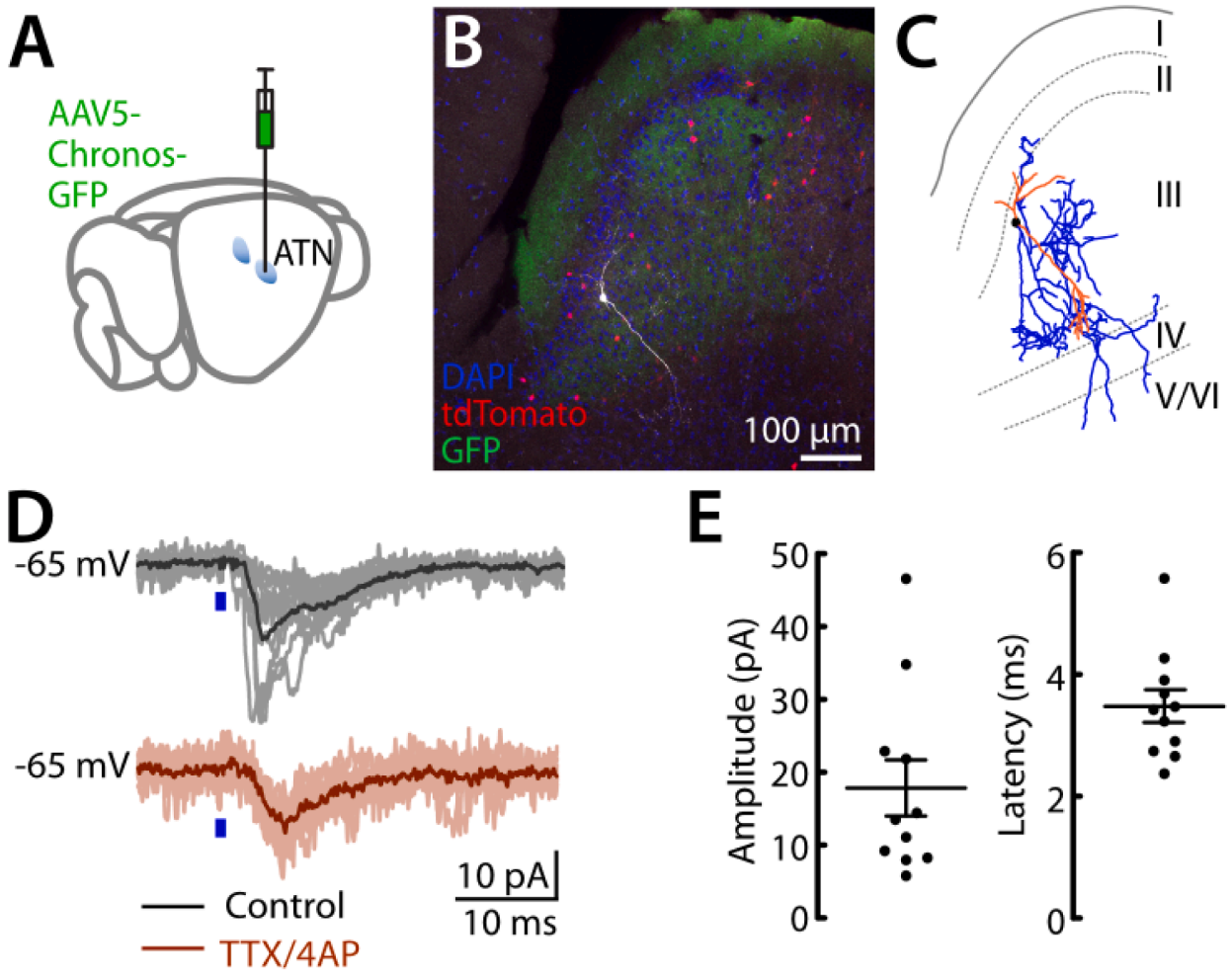

Fig. 5. Anterior thalamic fibers excite VIP interneurons in superficial layers. A) AAV5 viral vector was injected in ATN to express the channelrhodopsin Chronos fused with GFP in thalamic afferents to the presubiculum. B) Presubicular horizontal slice with a biocytin-filled VIP interneuron (white) in layer 3. DAPI in blue. tdTomato+ neurons in red. ATN axons in superficial layers in green. C) Neurolucida reconstruction of axons (blue) and dendrites (red) of this VIP interneuron of Cluster 3. D) Light-evoked EPSCs at holding potential of −65 mV in control conditions (black, top) and in the presence of TTX (1 µM) and 4-AP (100 µM) in the bath solution (red, bottom). Blue bars indicate photostimulation. E) EPSC amplitudes (left) and latencies (right) from n = 11 VIP interneurons (mean ± SEM). (For interpretation of the references to color in this figure legend, the reader is referred to the web version of this article.)

connection is monosynaptic (Fig. 5C, n = 11).

We next compared the dynamics of firing during repetitive ATN fiber stimulation with low light intensities (0.1–0.5 mW; Fig. 6A-C). The tested frequencies ranged from 10 to 70 Hz. The first light pulse in a train very often failed to evoke EPSPs, or, the EPSPs were too small to induce spiking responses. The following simulations led to more reliable EPSP generation that could reach firing threshold and thus initiate action potentials. We quantified the failure rate for EPSP initiation for the first and second pulse of stimulation. Failures occurred with a 49 % probability for the first pulse (success rate, 0.51 ± 0.06) and 22 % probability for the second pulse (success rate, 0.78 ± 0.05; Fig. 6D). Across all frequencies, failures were significantly reduced at the second pulse of stimulation. The probability to initiate firing in VIP interneurons increased for later pulses in a train, and in particular for higher stimulation frequencies that favored EPSP summation. Spiking probabilities were highest for the sixth pulse at 30 Hz and the seventh pulse at 10 Hz and at 70 Hz (n = 11 neurons from 3 animals, Fig. 6E). High spiking probability was maintained during the last 5 pulses. Strongly facilitating dynamics were apparent for 30 Hz and 70 Hz stimulations: a significant facilitation was observed for the sixth and seventh pulse at 30 Hz and 70 Hz stimulation (Kruskal–Wallis and Dunn's multiple comparison post hoc test, *<p 0.05 test; Fig. 6E) compared to the first pulse. These data indicate that ATN inputs directly connect VIP interneurons that integrate these inputs with facilitating dynamics.

Recording VIP interneurons at a slightly depolarized holding potential while stimulating afferent thalamic fibers let us distinguish direct excitatory and indirect inhibitory subthreshold components of the synaptic responses. A single stimulation could induce either an EPSP only, an IPSP only, or a sequence of both (Fig. 6F, G). For low-intensity light stimulation, 69 % of trials were successful to initiate a detectable postsynaptic response, while the remaining 31 % of trials failed to do so (single stimulation or first stimulation in a train; n = 11 cells, Fig. 6G). The majority of all trials resulted either in postsynaptic excitation (55 ± 11 %) or inhibition (52 ± 16 %). Occasionally a sequence of excitatory followed by inhibitory postsynaptic potentials (6 ± 0 %) was induced.

The typical excitatory postsynaptic responses occurred with a very short latency, as measured either from EPSCs (Fig. 5D) or EPSPs (Fig. 6), as expected for a direct monosynaptic connection. The latencies for inhibitory postsynaptic events were more variable. We distinguish early inhibition with short onset latencies (early I, 4.9 ± 0.6 ms, light green histogram), and inhibition with somewhat longer onset latencies (late I, 6.6 ± 0.7 ms, dark blue histogram; Fig. 6H,I). Inhibition could be preceded by an excitatory event in the case of excitatory-inhibitory

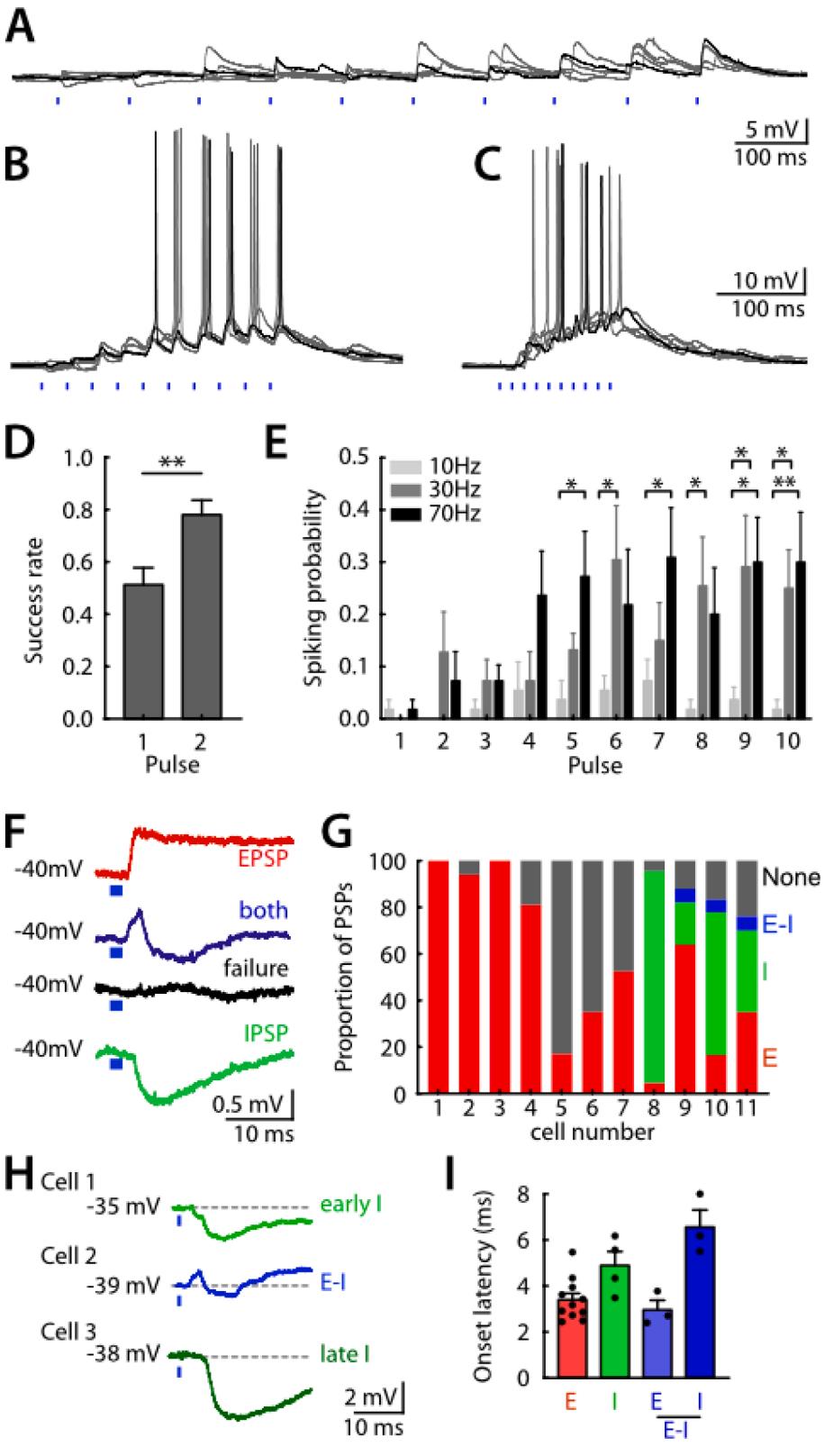

(caption on next page)

Fig. 6. VIP interneuron recruitment following optical stimulation of Chronos-expressing ATN fibers. A, B, C) Membrane potential responses of a VIP interneuron to photostimulation of ATN axons at different frequencies. D) The first and second light pulses in a train often do not lead to detectable EPSPs (success rates calculated from 5 trials in n = 11 VIP interneurons. Wilcoxon matched-pairs signed rank test, $^{**}p < 0.01$. E) AP spiking probabilities following 10 repetitive stimulations at 10 Hz (light grey), 30 Hz (dark grey) and 70 Hz (black). Data are shown as mean ± SEM. Kruskal–Wallis and Dunn's multiple comparison post hoc test, *p 0.05; Two-way ANOVA, $^{*}p < 0.05$. F) Individual unitary PSPs recorded from a VIP interneuron (holding potential, −40 mV). Low intensity photostimulation of ATN fibers evoked postsynaptic responses that were either EPSP-only (red), IPSP-only (green), biphasic (blue) PSPs or failures (grey) in this VIP interneuron. G) Summary of postsynaptic responses to single pulses of low intensity photostimulation grouped as EPSP-only (red), IPSP-only (green), biphasic (blue) or failures (grey) for each of the recorded VIP interneurons. Neurons #1, #4 and #5 and #10 are cluster 2 interneurons. Neurons #2, #3, #6, #7, #8, #9 and #11 are from cluster 3. H) Inhibitory postsynaptic potentials occurred either as early IPSPs (early I, light green), as sequence of excitation-inhibition (E-I, blue) or, as late IPSPs (late I, darker green). I) Onset latencies of EPSPs from 11 neurons, and of IPSPs from a subset of n = 4 VIP interneurons. (For interpretation of the references to color in this figure legend, the reader is referred to the web version of this article.)

postsynaptic responses (E-I). Excitatory events had very short latencies when occurring alone (excitation only, 3.4 ± 0.3 ms) and when followed by an inhibitory response (excitatory-inhibitory response, E-I, 2.9 ± 0.4 ms; Fig. 6H, I).

Discussion

Here we report for the first time the layer distribution, morphologies, and electrophysiological properties of VIP interneurons in the presubiculum. We find a high specificity of the VIPcre driver mouse line, validated by VIP immunoreactivity of tdTomato labeled neurons. Presubicular VIP interneurons are highly excitable. They can be divided into groups based on their electrophysiological properties. At least a subset of VIP interneurons receives anterior thalamic input, which may shape HD signal integration and updating via disinhibition.

VIPcre mice have been used previously for studies on other hippocampal regions. Our result on the overlap between tdTomato-positive cells and VIP immunoreactivity was similar to that reported for hippocampal area CA1 and dentate gyrus (Wei et al., 2021), suggesting that this mouse line is well-suited for studying VIP interneurons in the hippocampus and in the presubicular HD cortex. The quantification of the layer distribution and density of VIP interneurons in the PrS shows an absence of VIP interneurons in layer I, which is a largely cell free layer (Simonnet et al., 2013). Layer II has an overall high cell density, and the highest density of VIP interneurons per volume in the PrS. In layer III, the density of VIP interneurons decreased, and further so in deep layers IV and V/VI. Presubicular VIP cell density is similar to that of VIP cells in the barrel cortex showing a clear peak in superficial layer II/III (Prönneke et al., 2015). This layer distribution of VIP cells contrasts with that of SST interneurons, that are more densely distributed in the deep layers. It is more similar to that of PV interneurons with a high density in layer III (Nassar et al., 2015). The layer distribution of VIP interneuron somata may not predict their connectivity. Indeed, we show in Fig. 1 that the axons of VIP cells mostly ramify in layer III and to a lesser extent in the deep layers.

VIP interneurons co-express other neurochemical markers. Previous work from our group found a substantial portion of all GABAergic neurons (9 %) co-expressing VIP and calretinin (CR) in the presubiculum (Lofredi, 2017). The majority of VIP+ cells (78 %) were also positive for CR, and most numerous in layers II and III. VIP+/CR+ co-expressing neurons also exist in other cortical areas and in the hippocampus (termed type 3 interneuron-specific interneurons (IS3), Guet-McCreight et al., 2020; Francavilla et al., 2015; see also Kawaguchi and Kubota, 1997; Gonchar et al., 2008; Xu et al., 2010; Somogyi and Klausberger, 2005). VIP+/CR+ interneurons in the hippocampus are vertical mono- or bipolar cells, mediating disinhibition, while VIP+/CCK+ basket cells are multipolar and target the perisomatic region of CA1 pyramidal neurons (Acsády et al., 1996, Tyan et al., 2014). VIP interneuron co-expression of either CR or CCK appears to be exclusive (Kawaguchi and Kubota, 1997; Xu et al, 2010; Somogyi and Klausberger 2005; Huang and Paul, 2019). Sparsely distributed throughout the cortex are VIP interneurons (0.5 %) that co-express choline acetyl-transferase (ChAT; von Engelhardt et al., 2007; Dudai et al., 2020). We speculate that the groups of VIP interneurons in the presubiculum described here might correspond to distinct molecular profiles of VIP interneurons.

The classification of interneurons relies on multiple criteria, including electrophysiological properties, and also morphology, molecular markers and their transcriptome (Parra et al., 1998; Markram et al., 2004; Petilla Interneuron Nomenclature Group, 2008; Huang and Paul, 2019; Gouwens et al., 2020). Several electrophysiological parameters may be obtained from the voltage responses of neurons to hyperpolarizing and depolarizing current steps (Nassar et al., 2015; Simonnet et al., 2013). Here, we used an unsupervised cluster analysis (Ward, 1963) based only on electrophysiological parameters to search for potential subpopulations of VIP interneurons. Our analysis revealed two groups of VIP interneurons that segregated from a cluster containing the reference group of presubicular pyramidal cells, with distinct firing patterns and action potential shapes. A third group of VIP interneurons clustered together with the pyramidal cells (Fig. 3). The input resistance values were very high in all groups of presubicular VIP interneurons (in particular in Clusters 1 and 2). Indeed, input resistance may vary depending on the holding membrane potential it is measured at. Here it was calculated around −65 mV (in a voltage range between −55 mV and −75 mV), which is the region of the highest resistance (cf Fig. 3E). Therefore, the presubicular VIP interneurons in Cluster 1 and 2 may be similar to VIP+/CR+ neocortical and hippocampal IS3 interneurons, that are identified by a high input resistance, excitability and irregularly spiking firing pattern (Porter et al., 1998; Tyan et al., 2014; Miyoshi et al., 2010; Badrinarayanan et al., 2021). Presubicular VIP interneurons may also possess these combined features. They differ from VIP+/CCK+ basket cells in the hippocampus and from long range projecting hippocampal VIP interneurons, as those have a lower input resistance (Chamberland et al., 2010; Tyan et al., 2014; Francavilla et al., 2018). Those might be comparable to the group of VIP interneurons in cluster 3. Many presubicular VIP interneurons did not sustain firing over the 800 ms depolarization, with irregular firing patterns similar to the morpho-electric transcriptomic Vip-MET type 2 to 5 of visual cortex (Gouwens et al., 2020). The membrane potential in presubicular VIP interneurons (overall average, −55 ± 1 mV) was relatively depolarized, similar to cortical irregular spiking VIP interneurons (Miyoshi et al., 2010) and to VIP interneurons in the medial entorhinal cortex (Badrinarayanan et al., 2021). Comparable RMP values were also found in Martinotti type SST interneurons (Simonnet et al., 2017, Nassar et al., 2018). We note that the variance of electrical properties within our VIP interneuron groups is relatively high, pointing to possible additional subdivisions and heterogeneity within the subtypes. The low number of reconstructed VIP interneurons does not allow correlating the electrophysiological features of each group with particular morphological traits. More reconstructions are needed to determine if VIP interneuron heterogeneity of electrophysiological properties correlates with morphological features.

Across the cortex and the hippocampus, GABAergic interneurons with various intrinsic properties, connectivities and synaptic dynamics are known to shape circuit operations (Rudy et al., 2011; Pfeffer et al., 2013; Tremblay et al., 2016). Inhibitory-to-inhibitory synaptic interactions among VIP, SST, and PV interneurons maintain a balance between inhibition and disinhibition, and participate in stabilizing cortical circuit functions (Ozeki et al., 2009; Litwin-Kumar et al., 2016;

Millman et al., 2020; Sadeh and Clopath, 2021). The activity of VIP interneurons can be regulated through cholinergic inputs, according to context. They become activated in relation to locomotion, arousal, surprise and the expectation of reward (Lee et al., 2013; Fu et al., 2014; Pakan et al., 2016; Dipoppa et al., 2018; Ramamurthy et al., 2023). VIP interneurons mediate gain control of cortical activity via disinhibition, as a function of behavioral states (Fu et al., 2014). In visual cortex, VIP interneurons inhibit SST interneurons in particular, altering state-dependent modulation of cortical activity and visual perception (Ferguson et al., 2023). In barrel cortex, VIP interneurons mediate disinhibition and gate plasticity of intracortical synapses, following their activation by high-order thalamic input (Williams and Holtmaat, 2019). In the hippocampus, VIP interneuron mediated disinhibition supports spatial reward learning (Turi et al., 2019).

In the presubicular HD cortex, the excitatory-inhibitory interactions between pyramidal neurons and Martinotti type SST interneurons stabilize the HD attractor network locally (Simonnet et al., 2017). What could be the functional role of VIP interneurons? Our data show that at least two groups of presubicular VIP interneurons receive direct thalamic input, and the facilitating recruitment of VIP interneurons matches that of Martinotti type interneurons (which are indirectly recruited, Simonnet et al., 2017). We speculate that VIP interneurons may become active when the internal prediction of the HD signal does not match the current landmark context signaled by retrosplenial input (Van Groen and Wyss, 1990; Vann et al., 2009; Vogt and Miller, 1983). VIP interneuron inhibition of SST interneurons would then destabilize the bump state, and weaken the attractor, which may be a necessary condition for HD updating. And because SST interneurons synapse on the dendrites of pyramidal neurons, VIP disinhibition may also gate dendritic integration of thalamic and retrosplenial synaptic excitation in pyramidal neurons (Miles et al., 1996; Richevaux et al., 2023). More knowledge on the microcircuit connectivity and input–output characteristics of VIP interneurons will be necessary to infer how they govern circuit computation. Different subpopulations of VIP interneurons might differentially target principal cells or other interneurons, mediating inhibitory or disinhibitory operations. Simultaneous double recording of VIP interneurons together with pyramidal cells, or PV or SST interneurons could address this point. Deciphering the role of VIP interneurons for the presubicular HD circuit function will require the manipulation or the direct recording of identified VIP interneurons *in vivo*. In the future, experimental access to genetically defined VIP interneuron subtypes will be helpful. Enhancer-driven viral vectors (Nair et al., 2020) promise to enable subtype and circuit specific functional studies.

Author contributions

Conception and design of the work: MN, LR, DF. Acquisition, analysis or interpretation of data: MN, LR, DL, DT, EM, DF. Drafting the work or revising it critically: MN, LR, DF. Final approval of the version to be published: MN, LR, DL, DT, EM, DF.

CRediT authorship contribution statement

Mérie Nassar: Conceptualization, Data curation, Formal analysis, Investigation, Methodology, Supervision, Validation, Visualization, Writing – original draft, Writing – review & editing. **Louis Richevaux:** Conceptualization, Data curation, Formal analysis, Investigation, Methodology, Supervision, Validation, Visualization, Writing – original draft, Writing – review & editing. **Dongkyun Lim:** Investigation. **Dario Tayupo:** Investigation. **Erwan Martin:** Investigation. **Desdemona Fricker:** Conceptualization, Data curation, Funding acquisition, Methodology, Project administration, Supervision, Validation, Writing – original draft, Writing – review & editing.

Declaration of Competing Interest

The authors declare that they have no known competing financial interests or personal relationships that could have appeared to influence the work reported in this paper.

Acknowledgements

We benefited from support by the BioMedTech Facilities at Université Paris Cité (Institut National de la Santé et de la Recherche Médicale Unité S36/Unité Mixte de Service 2009). We acknowledge technical assistance from Fabrice Licata from the UPC Microscopy platform. This work was financially supported by the Centre National de la Recherche Scientifique and the Université Paris Cité. DF received funding from the Agence Nationale de la Recherche from the ERA-NET NEURON Program (ANR-20-NEUR-0005 VELOSO) and the FLAG-ERA HBP Program (ANR-21-HBPR-0002 VIPattract).

Appendix A. Supplementary data

Supplementary data to this article can be found online at https://doi.org/10.1016/j.neuroscience.2024.09.032.

References

Acsády, L., Görcs, T.J., Freund, T.F., 1996. Different populations of vasoactive intestinal polypeptide-immunoreactive interneurons are specialized to control pyramidal cells or interneurons in the hippocampus. Neuroscience 73 (2), 317–334.

Apicella, A.J., Marchionni, I., 2022. VIP-expressing GABAergic neurons: disinhibitory vs. inhibitory motif and its role in communication across neocortical areas. Front. Cell. Neurosci. 16, 811484.

Badrinarayanan, S., Manseau, F., Williams, S., Brandon, M.P., 2021. A characterization of the electrophysiological and morphological properties of vasoactive intestinal peptide (VIP) interneurons in the medial entorhinal cortex (MEC). Front. Neural Circuits 15, 653116.

Boccara, C.N., Sargolini, F., Thoresen, V.H., Solstad, T., Witter, M.P., Moser, E.I., Moser, M.-B., 2010. Grid cells in pre- and parasubiculum. Nat. Neurosci. 13, 987–994.

Booker, S.A., Vida, I., 2019. Morphological diversity and connectivity of hippocampal interneurons. Cell Tissue Res. 373 (3), 619–641.

Chamberland, S., Salesse, C., Topolnik, D., Topolnik, L., 2010. Synapse-specific inhibitory control of hippocampal feedback inhibitory circuit. Front. Cell. Neurosci. 15 (4), 130.

Cruikshank, S.J., Urabe, H., Nurmikko, A.V., Connors, B.W., 2010. Pathway-specific feedforward circuits between thalamus and neocortex revealed by selective optical stimulation of axons. Neuron 65 (2), 230–245.

Dipoppa, M., Ranson, A., Krumin, M., Pachitariu, M., Carandini, M., Harris, K.D., 2018. Vision and locomotion shape the interactions between neuron types in mouse visual cortex. Neuron 98 (3), 602–615.e8.

Dudai, A., Yayon, N., Lerner, V., Tasaka, G.I., Deitcher, Y., Gorfine, K., Niederhoffer, N., Mizrahi, A., Soreq, H., London, M., 2020. Barrel cortex VIP/ChAT interneurons suppress sensory responses in vivo. PLoS Biol. 18 (2), e3000613.

Duszkiewicz, A.J., Orhan, P., Skromne Carrasco, S., Brown, E.H., Owczarek, E., Vite, G. R., Wood, E.R., Peyrache, A., 2024. Local origin of excitatory-inhibitory tuning equivalence in a cortical network. Nat. Neurosci. 27 (4), 782–792.

Ferguson, K.A., Salameh, J., Alba, C., Selwyn, H., Barnes, C., Lohani, S., Cardin, J.A., 2023. VIP interneurons regulate cortical size tuning and visual perception. Cell Rep. 03.14.532664.

Francavilla, R., Luo, X., Magnin, E., Tyan, L., Topolnik, L., 2015. Coordination of dendritic inhibition through local disinhibitory circuits. Front. Synaptic Neurosci. 7, 5. https://doi.org/10.3389/fnsyn.2015.00005.

Francavilla, R., Villette, V., Luo, X., Chamberland, S., Muñoz-Pino, E., Camiré, O., Wagner, K., Kis, V., Somogyi, P., Topolnik, L., 2018. Connectivity and network state dependent recruitment of long-range VIP-GABAergic neurons in the mouse hippocampus. Nat. Commun. 9 (1), 5043.

Fu, Y., Tucciarone, J.M., Espinosa, J.S., Sheng, N., Darcy, D.P., Nicoll, R.A., Huang, Z.J., Stryker, M.P., 2014. A cortical circuit for gain control by behavioral state. Cell 156 (6), 1139–1152.

Golowasch, J., Thomas, G., Taylor, A.L., Patel, A., Pineda, A., Khalil, C., Nadim, F., 2009. Membrane capacitance measurements revisited: dependence of capacitance value on measurement method in nonisopotential neurons. J. Neurophysiol. 102 (4), 2161–2175.

Gonchar, Y., Wang, Q., Burkhalter, A., 2008. Multiple distinct subtypes of GABAergic neurons in mouse visual cortex identified by triple immunostaining. Front. Neuroanat. 1, 3.

Gouwens, N.W., Sorensen, S.A., Baftizadeh, F., Budzillo, A., Lee, B.R., Jarsky, T., Alfiler, L., Baker, K., Barkan, E., Berry, K., Bertagnolli, D., Bickley, K., Bomben, J., Braun, T., Brouner, K., Casper, T., Crichton, K., Daigle, T.L., Dalley, R., de Frates, R.

A., Dee, N., Desta, T., Lee, S.D., Dotson, N., Egdorf, T., Ellingwood, L., Enstrom, R., Esposito, L., Farrell, C., Feng, D., Fong, O., Gala, R., Gamlin, C., Gary, A., Glandon, A., Goldy, J., Gorham, M., Graybuck, L., Gu, H., Hadley, K., Hawrylycz, M. J., Henry, A.M., Hill, D., Hupp, M., Kebede, S., Kim, T.K., Kim, L., Kroll, M., Lee, C., Link, K.E., Mallory, M., Mann, R., Maxwell, M., McGraw, M., McMillen, D., Mukora, A., Ng, L., Ng, L., Ngo, K., Nicovich, P.R., Oldre, A., Park, D., Peng, H., Penn, O., Pham, T., Pom, A., Popović, Z., Potekhina, L., Rajanbabu, R., Ransford, S., Reid, D., Rimorin, C., Robertson, M., Ronellenfitch, K., Ruiz, A., Sandman, D., Smith, K., Sulc, J., Sunkin, S.M., Szafer, A., Tieu, M., Torkelson, A., Trinh, J., Tung, H., Wakeman, W., Ward, K., Williams, G., Zhou, Z., Ting, J.T., Arkhipov, A., Sümbül, U., Lein, E.S., Koch, C., Yao, Z., Tasic, B., Berg, J., Murphy, G.J., Zeng, H., 2020. Integrated morphoelectric and transcriptomic classification of cortical GABAergic cells. Cell 183 (4), 935–953.e19.

Guet-McCreight, A., Skinner, F.K., Topolnik, L., 2020. Common principles in functional organization of VIP/calretinin cell-driven disinhibitory circuits across cortical areas. Front. Neural Circuits 14, 32.

Hajos, N., Acsady, L., Freund, T.F., 1996. Target selectivity and neurochemical characteristics of VIP-immunoreactive interneurons in the rat dentate gyrus. Eur. J. Neurosci. 8 (7), 1415–1431.

Huang, L.W., Simonnet, J., Nassar, M., Richevaux, L., Lofredi, R., Fricker, D., 2017. Laminar localization and projection-specific properties of presubicular neurons targeting the lateral mammillary nucleus, thalamus, or medial entorhinal cortex. eNeuro 4:ENEURO.0370-16.2017.

Huang, Z.J., Paul, A., 2019. The diversity of GABAergic neurons and neural communication elements. Nat. Rev. Neurosci. 20, 563–1557.

Jackson, J., Karnani, M.M., Zemelman, B.V., Burdakov, D., Lee, A.K., 2018. Inhibitory control of prefrontal cortex by the claustrum. Neuron 99 (5), 1029–1039.e4.

Karnani, M.M., Agetsuma, M., Yuste, R., 2014. A blanket of inhibition: functional inferences from dense inhibitory connectivity. Curr. Opin. Neurobiol. 26, 96–102.

Karnani, M.M., Jackson, J., 2018. Interneuron cooperativity in cortical circuits. Neuroscientist 24 (4), 329–341.

Kawaguchi, Y., Kubota, Y., 1997. GABAergic cell subtypes and their synaptic connections in rat frontal cortex. Cereb. Cortex 7 (6), 476–486.

Kepecs, A., Fishell, G., 2016. Interneuron cell types are fit to function. Nature 505 (7483), 318–326.

Klapoetke, N.C., Murata, Y., Kim, S.S., Pulver, S.R., Birdsey-Benson, A., Cho, Y.K., Morimoto, T.K., Chuong, A.S., Carpenter, E.J., Tian, Z., Wang, J., Xie, Y., Yan, Z., Zhang, Y., Chow, B.Y., Surek, B., Melkonian, M., Jayaraman, V., Constantine-Paton, M., Wong, G.K., Boyden, E.S., 2014. Independent optical excitation of distinct neural populations. Nat. Methods 11 (3), 338–346.

Krabbe, S., Paradiso, E., d'Aquin, S., Bitterman, Y., Courtin, J., Xu, C., Yonehara, K., Markovic, M., Müller, C., Eichlisberger, T., Gründemann, J., Ferraguti, F., Lüthi, A., 2019. Adaptive disinhibitory gating by VIP interneurons permits associative learning. Nat. Neurosci. 22 (11), 1834–1843.

Langston, R.F., Ainge, J.A., Couey, J.J., Canto, C.B., Bjerknes, T.L., Witter, M.P., Moser, E.I., Moser, M.B., 2010. Development of the spatial representation system in the rat. Science 328 (5985), 1576–1580.

Lee, S., Kruglikov, I., Huang, Z.J., Fishell, G., Rudy, B., 2013. A disinhibitory circuit mediates motor integration in the somatosensory cortex. Nat. Neurosci. 16 (11), 1662–1670.

Litwin-Kumar, A., Rosenbaum, R., Doiron, B., 2016. Inhibitory stabilization and visual coding in cortical circuits with multiple interneuron subtypes. J. Neurophysiol. 115 (3), 1399–1409.

Lofredi, R., 2017. Characterization of inhibitory and projection specific neurons of the presubiculum. Dissertation, Repositorium der Freien Universität Berlin.

Madisen, L., Zwingman, T.A., Sunkin, S.M., Oh, S.W., Zariwala, H.A., Gu, H., Ng, L.L., Palmiter, R.D., Hawrylycz, M.J., Jones, A.R., Lein, E.S., Zeng, H., 2010. A robust and high-throughput Cre reporting and characterization system for the whole mouse brain. Nat. Neurosci. 13 (1), 133–140.

Mao, T., Kusefoglu, D., Hooks, B.M., Huber, D., Petreanu, L., Svoboda, K., 2011. Long-range neuronal circuits underlying the interaction between sensory and motor cortex. Neuron 72 (1), 111–123.

Markram, H., Toledo-Rodriguez, M., Wang, Y., Gupta, A., Silberberg, G., Wu, C., 2004. Interneurons of the neocortical inhibitory system. Nat. Rev. Neurosci. 5 (10), 793–807.

Mathon, B., Nassar, M., Simonnet, J., Le Duigou, C., Clemenceau, S., Miles, R., Fricker, D., 2015. Increasing the effectiveness of intracerebral injections in adult and neonatal mice: a neurosurgical point of view. Neurosci. Bull. 31 (6), 685–696.

McNaughton, B.L., Battaglia, F.P., Jensen, O., Moser, E.I., Moser, M.-B., 2006. Path integration and the neural basis of the "cognitive map". Nat. Rev. Neurosci. 7, 663–678.

Miles, R., Tóth, K., Gulyás, A.I., Hájos, N., Freund, T.F., 1996 Apr. Differences between somatic and dendritic inhibition in the hippocampus. Neuron 16 (4), 815–823.

Millman, D.J., Ocker, G.K., Caldejon, S., Kato, I., Larkin, J.D., Lee, E.K., Luviano, J., Nayan, C., Nguyen, T.V., North, K., Seid, S., White, C., Lecoq, J., Reid, C., Buice, M. A., de Vries, S.E., 2020. VIP interneurons in mouse primary visual cortex selectively enhance responses to weak but specific stimuli. Elife 9, e55130.

Miyoshi, G., Hjerling-Leffler, J., Karayannis, T., Sousa, V.H., Butt, S.J., Battiste, J., Johnson, J.E., Machold, R.P., Fishell, G., 2010. Genetic fate mapping reveals that the caudal ganglionic eminence produces a large and diverse population of superficial cortical interneurons. J. Neurosci. 30 (5), 1582–1594.

Nair, R.R., Blankvoort, S., Lagartos, M.J., Kentros, C., 2020. Enhancer-driven gene expression (EDGE) enables the generation of viral vectors specific to neuronal subtypes. In: iScience, 23.

Nassar, M., Simonnet, J., Lofredi, R., Cohen, I., Savary, E., Yanagawa, Y., Miles, R., Fricker, D., 2015. Diversity and overlap of parvalbumin and somatostatin expressing interneurons in mouse presubiculum. Front. Neural Circuits 9, 20.

Nassar, M., Simonnet, J., Huang, L.-W., Mathon, B., Cohen, I., Bendels, M.H.K., Beraneck, M., Miles, R., Fricker, D., 2018. Anterior thalamic excitation and feedforward inhibition of presubicular neurons projecting to medial entorhinal cortex. Jneurosci 38, 6411–6425.

Ozeki, H., Finn, I.M., Schaffer, E.S., Miller, K.D., Ferster, D., 2009. Inhibitory stabilization of the cortical network underlies visual surround suppression. Neuron 62 (4), 578–592.

Pakan, J.M., Lowe, S.C., Dylda, E., Keemink, S.W., Currie, S.P., Coutts, C.A., Rochefort, N.L., 2016. Behavioral-state modulation of inhibition is context-dependent and cell type specific in mouse visual cortex. Elife 5, e14985.

Parra, P., Gulyás, A.I., Miles, R., 1998. How many subtypes of inhibitory cells in the hippocampus? Neuron 20 (5), 983–993.

Peng, Y., Barreda Tomás, F.J., Klisch, C., Vida, I., Geiger, J.R.P., 2017. Layer-specific organization of local excitatory and inhibitory synaptic connectivity in the rat Presubiculum. Cereb. Cortex 27 (4), 2435–2452.

Petilla Interneuron Nomenclature Group, Ascoli, G.A., Alonso-Nanclares, L., Anderson, S. A., Barrionuevo, G., Benavides-Piccione, R., Burkhalter, A., Buzsáki, G., Cauli, B., Defelipe, J., Fairén, A., Feldmeyer, D., Fishell, G., Fregnac, Y., Freund, T.F., Gardner, D., Gardner, E.P., Goldberg, J.H., Helmstaedter, M., Hestrin, S., Karube, F., Kisvárday, Z.F., Lambolez, B., Lewis, D.A., Marin, O., Markram, H., Muñoz, A., Packer, A., Petersen, C.C., Rockland, K.S., Rossier, J., Rudy, B., Somogyi, P., Staiger, J.F., Tamas, G., Thomson, A.M., Toledo-Rodriguez, M., Wang, Y., West, D.C., Yuste, R., 2008. Petilla terminology: nomenclature of features of GABAergic interneurons of the cerebral cortex. Nat. Rev. Neurosci. 9 (7), 557–568.

Pfeffer, C.K., Xue, M., He, M., Huang, Z.J., Scanziani, M., 2013. Inhibition of inhibition in visual cortex: the logic of connections between molecularly distinct interneurons. Nat. Neurosci. 16 (8), 1068–1076.

Pi, H.J., Hangya, B., Kvitsiani, D., Sanders, J.I., Huang, Z.J., Kepecs, A., 2013. Cortical interneurons that specialize in disinhibitory control. Nature 503 (7477), 521–524.

Porter, J.T., Cauli, B., Staiger, J.F., Lambolez, B., Rossier, J., Audinat, E., 1998. Properties of bipolar VIPergic interneurons and their excitation by pyramidal neurons in the rat neocortex. Eur. J. Neurosci. 10 (12), 3617–3628.

Preston-Ferrer, P., Coletta, S., Frey, M., Burgalossi, A., 2016. Anatomical organization of presubicular head-direction circuits. In: eLife, 5.

Prönneke, A., Scheuer, B., Wagener, R.J., Möck, M., Witte, M., Staiger, J.F., 2015. Characterizing VIP Neurons in the Barrel Cortex of VIPcre/tdTomato Mice Reveals Layer-Specific Differences. Cereb. Cortex 25, 4854–4868.

Ramamurthy, D.L., Chen, A., Zhou, J., Park, C., Huang, P.C., Bharghavan, P., Krishna, G., Liu, J., Casale, K., Feldman, D.E., 2023. VIP interneurons in sensory cortex encode sensory and action signals but not direct reward signals. Curr. Biol. 18:S0960-9822 (23)00872-2.

Richevaux, L., Lim, D., Nassar, M., Dias Rodrigues, L., Mauthe, C., Cohen, I., Sol-Foulon, N., Fricker, D., 2023. Projection-specific integration of convergent thalamic and retrosplenial signals in the presubicular head direction cortex. eLife 12:RP92443.

Rudy, B., Fishell, G., Lee, S., Hjerling-Leffler, J., 2011. Three groups of interneurons account for nearly 100% of neocortical GABAergic neurons. Dev. Neurobiol. 71 (1), 45–61.

Sadeh, S., Clopath, C., 2021. Inhibitory stabilization and cortical computation. Nat. Rev. Neurosci. 22 (1), 21–37.

Simonnet, J., Eugène, E., Cohen, I., Miles, R., Fricker, D., 2013. Cellular neuroanatomy of rat presubiculum. Eur J Neuriosci 37, 583–597.

Simonnet, J., Fricker, D., 2018. Cellular components and circuitry of the presubiculum and its functional role in the head direction system. Cell Tissue Res. 373 (3), 541–556.

Simonnet, J., Nassar, M., Stella, F., Cohen, I., Mathon, B., Boccara, C.N., Miles, R., Fricker, D., 2017. Activity dependent feedback inhibition may maintain head direction signals in mouse presubiculum. Nat. Commun. 8, 16032.

Somogyi, P., Klausberger, T., 2005. Defined types of cortical interneuron structure space and spike timing in the hippocampus. J. Physiol. (Lond.) 562, 9–26.

Taniguchi, H., He, M., Wu, P., Kim, S., Paik, R., Sugino, K., Kvitsiani, D., Fu, Y., Lu, J., Lin, Y., Miyoshi, G., Shima, Y., Fishell, G., Nelson, S.B., Huang, Z.J., 2011. A resource of Cre driver lines for genetic targeting of GABAergic neurons in cerebral cortex. Neuron 71 (6), 995–1013.

Taube, J.S., Muller, R.U., Ranck, J.B., 1990. Head direction cells recorded from the postsubiculum in freely moving rats. J. Neurosci. 10, 420–435.

Topolnik, L., Tamboli, S., 2022. The role of inhibitory circuits in hippocampal memory processing. Nat. Rev. Neurosci. 23 (8), 476–492.

Tremblay, R., Lee, S., Rudy, B., 2016. GABAergic interneurons in the neocortex: from cellular properties to circuits. Neuron 91 (2), 260–292.

Tukker, J.J., Tang, Q., Burgalossi, A., Brecht, M., 2015. Head-directional tuning and theta modulation of anatomically identified neurons in the Presubiculum. J. Neurosci. 35, 15391–15395.

Turi, G.F., Li, W.K., Chavlis, S., Pandi, I., O'Hare, J., Priestley, J.B., Grosmark, A.D., Liao, Z., Ladow, M., Zhang, J.F., Zemelman, B.V., Poirazi, P., Losonczy, A., 2019. Vasoactive intestinal polypeptide-expressing interneurons in the hippocampus support goal-oriented spatial learning. Neuron 101 (6), 1150–1165.e8.

Tyan, L., Chamberland, S., Magnin, E., Camiré, O., Francavilla, R., David, L.S., Deisseroth, K., Topolnik, L., 2014 Mar 26. Dendritic inhibition provided by interneuron-specific cells controls the firing rate and timing of the hippocampal feedback inhibitory circuitry. J. Neurosci. 34 (13), 4534–4547. https://doi.org/10.1523/JNEUROSCI.3813-13.2014. PMID: 24671999; PMCID: PMC6608127.

Van Groen, T., Wyss, J.M., 1990. The connections of presubiculum and parasubiculum in the rat. Brain Res. 518, 227–243.

Vann, S.D., Aggleton, J.P., Maguire, E.A., 2009. What does the retrosplenial cortex do? Nat. Rev. Neurosci. 10, 792–802.

Vogt, B.A., Miller, M.W., 1983. Cortical connections between rat cingulate cortex and visual, motor, and postsubicular cortices. J. Comp. Neurol. 216, 192–210.

von Engelhardt, J., Eliava, M., Meyer, A.H., Rozov, A., Monyer, H., 2007. Functional characterization of intrinsic cholinergic interneurons in the cortex. J. Neurosci. 27, 5633–5642.

Ward, J.H., 1963. Hierarchical grouping to optimize an objective function. J. Am. Stat. Assoc. 58 (301), 236–244.

Wei, Y.T., Wu, J.W., Yeh, C.W., Shen, H.C., Wu, K.P., Vida, I., Lien, C.C., 2021. Morpho-physiological properties and connectivity of vasoactive intestinal polypeptide-expressing interneurons in the mouse hippocampal dentate gyrus. J. Comp. Neurol. 529 (10), 2658–2675.

Williams, L.E., Holtmaat, A., 2019. Higher-order thalamocortical inputs gate synaptic long-term potentiation via disinhibition. Neuron 101 (1), 91–102.e4.

Winter, S.S., Clark, B.J., Taube, J.S., 2015. Spatial navigation. Disruption of the head direction cell network impairs the parahippocampal grid cell signal. Science 347, 870–874.

Xu, X., Roby, K.D., Callaway, E.M., 2010. Immunochemical characterization of inhibitory mouse cortical neurons: three chemically distinct classes of inhibitory cells. J. Comp. Neurol. 518 (3), 389–404.